RSC Advances

PAPER

View Article Online
View Journal | View Issue



Cite this: *RSC Adv.*, 2016, **6**, 95793

# Methyl and phenyl substituent effects on the catalytic behavior of NHC ruthenium complexes†

Alessandra Perfetto,[a] Valerio Bertolasi,[b] Chiara Costabile,[a] Veronica Paradiso,[a] Tonino Caruso,[a] Pasquale Longo[a] and Fabia Grisi*[a]

Received 15th August 2016
Accepted 1st October 2016

DOI: 10.1039/c6ra20608e

www.rsc.org/advances

New second-generation ruthenium benzylidene and isopropoxybenzylidene catalysts bearing N-heterocyclic carbene (NHC) ligands with *o*-biphenyl groups at the N-atoms and *syn* methyl or phenyl groups on the backbone were obtained and their catalytic behaviors were compared to those of analogous *N*-*o*-tolyl catalysts in standard ring-closing metathesis (RCM) reactions. A pronounced difference in catalyst efficiency was observed depending on the nature of *ortho*-*N*-aryl substituents (methyl or phenyl). Notably, very impressive catalytic performances were exhibited by *N*-*o*-biphenyl complexes with a *syn* dimethyl backbone in the formation of di- and trisubstituted cycloalkenes. To rationalize catalytic results, methyl and phenyl substituent effects on the steric and electronic properties of NHC ligands were assessed through experimental and theoretical investigations involving ruthenium complexes as well as newly developed rhodium derivatives. Despite the different electron donor capacities of the examined carbenes, the steric differences shown by *N*-*o*-biphenyl and *N*-*o*-tolyl NHCs, although subtle, were found to be the key factor in addressing catalyst behavior.

## Introduction

N-heterocyclic carbenes (NHCs) are nowadays ubiquitous ligands in organometallic and coordination chemistry. Their unique steric and electronic features have made possible the development of effective metal catalysts for various applications, the most successful examples being in the field of ruthenium-catalyzed olefin metathesis.[1] Ruthenium complexes bearing NHC ligands, commonly referred to as second-generation catalysts, have demonstrated their superiority over first generation catalysts containing classical phosphine ligands exhibiting higher thermal stability, activity and selectivity (Chart 1).[2]

One of the major attractiveness of this class of complexes lies in the possibility of fine-tuning their catalytic properties by modifying the NHC stereoelectronics. Variation of the degree of backbone and/or *N*-aryl substitution of the NHC ligand has led to ruthenium catalysts especially competent for metathesis transformations involving hindered substrates.[3] In particular, the presence of bulky substituents on the backbone was found to improve catalyst stability[3c] limiting decomposition pathways due to C–H bond activation of *N*-aryl rings.[4] Furthermore, the symmetry of the NHC backbone associated with mono-*ortho*-substituted *N*-aryl groups has been recognized as a key parameter for successful ring-closing metathesis (RCM) reactions and, more interestingly, complexes with *syn* phenyl substituents on the backbone and *N*-*o*-tolyl rings has been identified as privileged catalysts in the most representative olefin metathesis

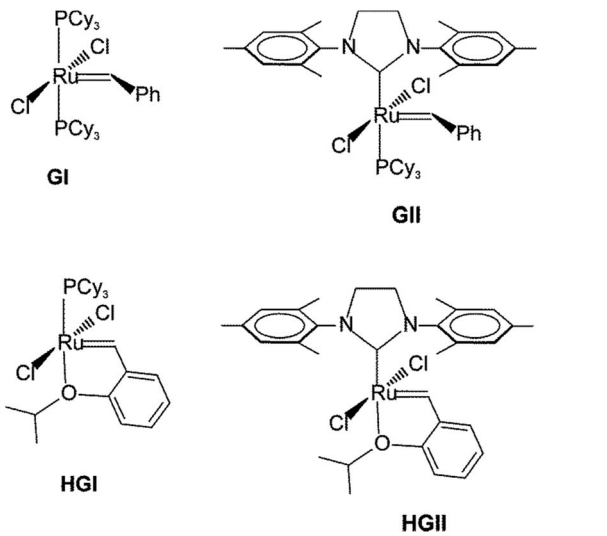


Chart 1 Grubbs' and Hoveyda–Grubbs' catalysts.

[a]*Dipartimento di Chimica e Biologia "Adolfo Zambelli", Università di Salerno, Via Giovanni Paolo II 132, I-84084 Fisciano, Salerno, Italy. E-mail: fgrisi@unisa.it*

[b]*Dipartimento di Scienze Chimiche e Farmaceutiche and Centro di Strutturistica Diffrattometrica, Università di Ferrara, Via L. Borsari 46, I-44121 Ferrara, Italy*

† Electronic supplementary information (ESI) available: Experimental procedures, figures giving NMR spectra of the new complexes **3**, **4**, **7** and **8**, cyclic voltammograms of **1–8**, tables and CIF files giving experimental details for complexes **7**, **21–24**, and computational details. CCDC 1483950–1483954. For ESI and crystallographic data in CIF or other electronic format see DOI: 10.1039/c6ra20608e

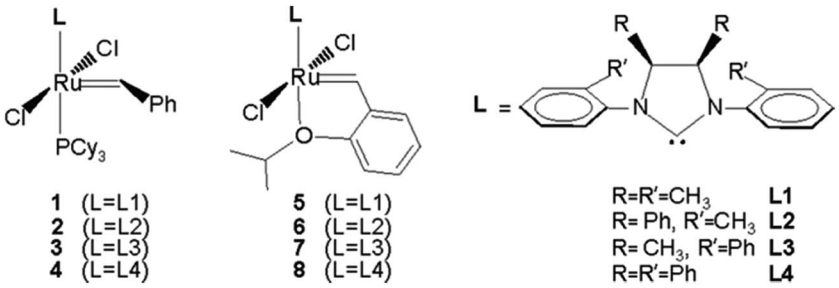


Chart 2 *syn*-NHC backbone substituted Ru catalysts.

processes (**1** and **5**, Chart 2).[3g,h] Indeed, the steric pressure of encumbered *syn* phenyl groups on the NHC backbone has been found to be an essential requirement to froze the most suitable NHC conformation (that is the one with *syn* oriented *N*-tolyl rings) for efficiently accomplishing metathesis reactions (**2** and **6**, Chart 2).[3g,h]

To gain a better understanding of the role played by the nature of *syn* NHC backbone substituents and of mono-*ortho*-substituted *N*-aryl groups in the achievement of highly performing catalysts, we thought to further investigate this type of substitution pattern employing different combinations of methyl and phenyl groups on the NHC ligand and evaluating their impact on the catalytic properties of the resulting catalysts. Therefore, in this study, we present the synthesis and characterization of new second generation Grubbs-type complexes **3**, **4** and Hoveyda–Grubbs-type complexes **7**, **8** (Chart 2), bearing methyl or phenyl substituents at the ring backbone associated with *o*-biphenyl groups at the nitrogen atoms, and we compare their behaviors in standard ring-closing metathesis reactions to those of already known complexes **1**, **2** and **5**, **6** having the same NHC backbone substitution and *o*-tolyl groups at the N atoms.[3e–h] The steric and electronic properties of the examined NHC ligands were assessed using both ruthenium and rhodium complexes and their possible correlations to observed catalyst reactivities are discussed, providing further advances in the understanding of which NHC characteristics are important for the rational design of RCM catalysts.

## Results and discussion

### Synthesis and characterization of Ru-based catalysts

Ru-catalysts **1**, **2**, **5** and **6** were prepared as earlier described.[3e–g] The synthesis of new complexes **3**, **4**, **7** and **8** were carried out as shown in Scheme 1. With regard to the synthesis of catalysts **3** and **7**, bearing *syn* methyl substituents on the NHC backbone, the chosen synthetic route involved the preparation of diamine **A**,[5] that was subsequently coupled with 2-bromobiphenyl by Pd-catalyzed reaction to give diarylated diamine **B**. Dihydroimidazolium salt **C** was obtained by treatment of **B** with HCl and then condensation with triethyl orthoformate. The corresponding free carbene generated *in situ* by treatment of **C** with hexamethyldisilazide (KHMDS) was reacted with **GI** to afford monophosphine complex **3** (33% yield)[7a] or, alternatively, with **HGI** to give phosphine-free complex **7** (72% yield). As for catalysts **4** and **8**, Pd-catalyzed diarylation of commercially available diamine **D** with 2-bromobiphenyl allowed to obtain **E**, that was then converted in the NHC ligand precursor **F** by reacting with triethyl orthoformate in the presence of ammonium tetrafluoroborate.[6] *In situ* deprotonation of **F** by potassium hexafluoro-*tert*-butoxide [$(CF_3)_2CH_3COK$] produced the desired free NHC that was treated with **GI** to afford complex **4** (66% yield). Phosphine-containing complex **4** was quantitatively transformed in the corresponding phosphine-free catalyst **8** by a cross-metathesis reaction with 2-isopropoxystyrene in the presence of CuCl as a phosphine scavenger. All the complexes were obtained as air- and moisture-stable solids after flash column chromatography and were fully characterized by 1D and 2D NMR spectroscopy.[7b]

As previously observed for analogous complexes,[3e–g] the preferred NHC conformation for phosphine-containing complexes **3** and **4** was assigned to be that with *syn*-oriented *N*-aryl groups pointing on the opposite sides of the *syn* NHC backbone substituents. For both complexes, variable temperature (VT) $^1$H and $^{31}$P NMR experiments revealed the presence of

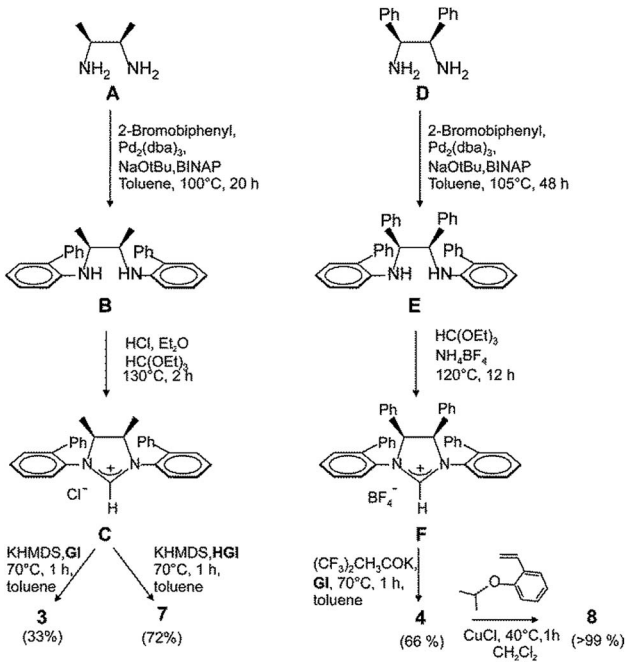


Scheme 1 Synthesis of new ruthenium complexes **3**, **4**, **7** and **8**.

 

two rotational isomers at low temperature, resulting from rotation around the benzylidene C–Ru bond or rotation about the Ru–NHC bond (see ESI†). Solution-state structures of phosphine-free complexes **7** and **8**, determined *via* NMR analysis, revealed the presence of a single isomer, corresponding to the species with the NHC ligand locked in the same conformation observed for **3** and **4**. The solid-state structure of **7** was unambiguously established by X-ray diffraction (Fig. 1). In this complex, the Ru center is penta-coordinated and adopts a distorted square pyramidal coordination geometry. The Cl atoms are *trans* oriented in the basal plane and the carbene C1 atom is in *trans* position with respect to the O1 oxygen of 2-iPrO substituent at the benzylidene ligand, which is almost coplanar with the NHC ring, being rotated by only 18.37(5)°.

This compound crystallizes in the centro-symmetric $P2_1/n$ space group with the NHC methyl groups in *cis* position with respect to C2–C3 bond. Accordingly the crystal contains a racemic mixture of both the enantiomers having opposite configurations (*RS* or *SR*) at the C2 and C3 asymmetric carbon atoms. The phenyl rings C14/C19 bonded to N1 and C26/C31 bonded to N2 are rotated by 53.68(6)° and 74.48(5)°, respectively, with respect to NHC ring. These conformations are mainly determined by short intramolecular interactions: H19⋯Ru1 = 2.71 Å and H4⋯C26 = 2.49 Å. The other structural parameters are very similar with respect to those observed in many other similar Hoveyda–Grubbs' second generation catalysts that differ only in the NHC substituents. Unfortunately, all the efforts of growing single crystals of **3**, **4** and **8** suitable for X-ray crystallographic analyses were unproductive.

## RCM catalytic behavior

The catalytic behaviors of new complexes **3**, **4**, **7** and **8** were investigated in standard RCM transformations, involving malonate (**9**, **13**, **17**) and tosylamine (**11**, **15**, **19**) derivatives with increasing steric hindrance, and compared to those of previously reported complexes **1**, **2**, **5** and **6**.[3e–h] All the reactions were conducted at 30 °C in $CD_2Cl_2$ with phosphine-containing complexes **1–4**, and at 60 °C in $C_6D_6$ with slow-initiating phosphine-free catalysts **5–8**. The conversion of each substrate to product was monitored over time by $^1$H NMR and the corresponding kinetic profiles are sketched in Fig. 2–4. Tables S1–S3 in the ESI† provide additional details on the examined RCM reactions.

As clearly shown by the kinetic profiles of the ring-closures of diethyl diallylmalonate (**9**) and diallyltosylamine (**11**) promoted by phosphine-containing complexes **1–4** (Fig. 2A and C), catalysts **3** and **4**, characterized by *o*-biphenyl *N*-substituents, displayed significantly higher activities than **1** and **2** bearing *o*-tolyl *N*-groups, rivaling those of the most efficient systems known up to now.[3f,9] Catalyst **3** with methyl groups on the backbone furnished quantitatively cycloalkenes **10** in 5 min and **12** in 3 min, performing slightly better than **4**, that needed 8 and 6 minutes to give the corresponding cyclic products in 95% and >98% conversion, respectively. Catalyst **2** was found to be slightly more active than **1**, nearly completing cyclization of **9** (95% conversion) and **11** (>98% conversion) in 18 and 22 minutes, respectively.

Differences in reactivity are much more difficult to notice for the same RCM reactions carried out in the presence of the corresponding phosphine-free catalysts **5–8** [10] (Fig. 2B and D), very likely as a consequence of the higher temperature employed to improve performances of this family of catalysts.[3f] However, also in this case the catalyst presenting methyls on the NHC backbone and *N*-*o*-biphenyl groups (**7**) outperformed the

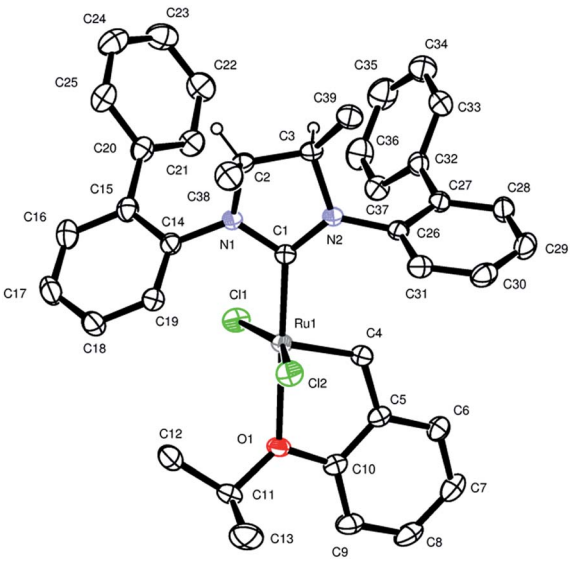


Fig. 1 ORTEP[8] view of **7** showing the thermal ellipsoids at 30% probability level. The H atoms, excluded those linked to C2 and C3 carbons of the NHC ring, have been omitted for sake of clarity.

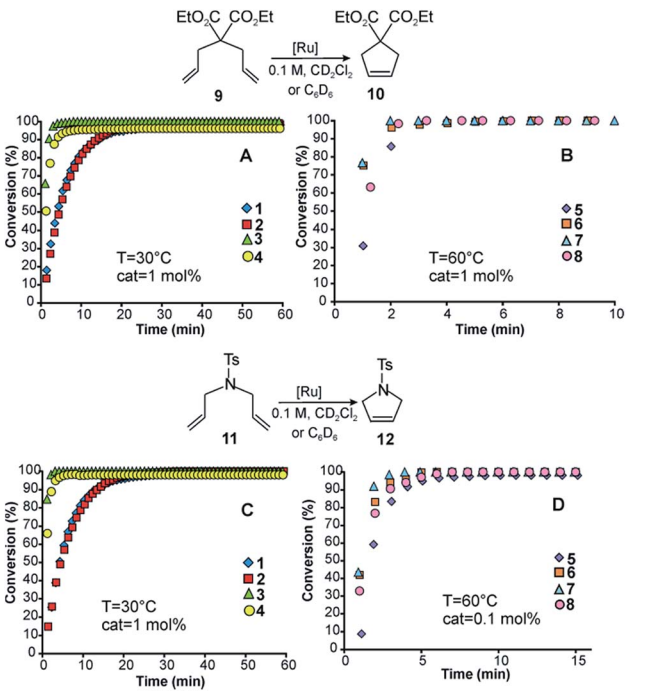


Fig. 2 Kinetic plots of the RCM of **9** and **11**.

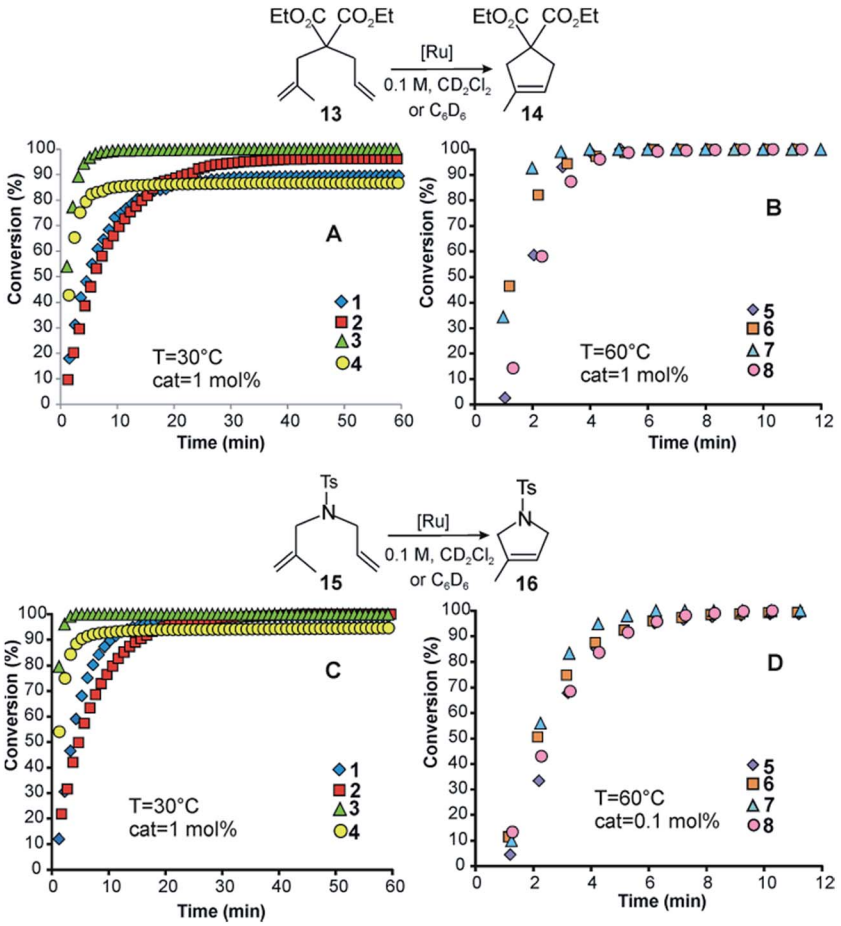


Fig. 3 Kinetic plots of the RCM of **13** and **15**.

other ones providing quantitatively the desired cyclic products **10** and **12** in 2 and 4 min, respectively.

The catalytic behavior of complexes **1–8** was then investigated in the RCM of more encumbered diolefins **13** and **15** (Fig. 3). As for phosphine-containing catalysts **1–4**, once again catalyst **3** exhibited the highest efficiency in forming cycloolefins **14** and **16** (>99% conversion in 9 and 4 min, respectively), emerging as the best performing system in this class of reaction up to now.[3f,9] On the other hand, catalyst **4**, despite the high initiation rate, gave final conversions slightly slower than those of catalysts **1** and **2**. The minor efficiency observed for **4** is likely due to a higher decomposition rate of the catalyst, as suggested by the analysis of the slope of the corresponding curves in Fig. 3A and C.

The ring-closures of **13** and **15** promoted by phosphine-free Ru-catalysts **5–8** displayed the same reactivity trend observed in the previous RCM, with only marginal deviations. Again, catalyst **7**, possessing *N*-*o*-biphenyl groups and *syn* dimethyl backbone, turned out to be the most active catalyst in both the transformations.

In the challenging RCM of sterically encumbered diolefins **17** and **19** (Fig. 4), more marked reactivity differences among catalysts **1–4** emerged and, in contrast to the previous results, the catalytic performances of complexes **3** and **4** with bulkier *N*-*o*-biphenyl substituents were inverted with respect to those of complexes **1** and **2**. As depicted in Fig. 4A, in the RCM of malonate derivative **17** complexes **1–4** exhibited nearly identical profiles at the beginning of the reaction. Their behaviors differentiated after roughly the first five minutes, when for catalysts **3** and **4** a strong decrease of reaction rate was observed, and plateau conversion values of 61% and 45% were respectively reached. In the easier RCM of tosyl derivative **19**, catalysts **3** and **4** gave better performances than in the previous cyclization, leading to 82% and 61% conversion respectively (Fig. 4C). Once again they proved to be less efficient than catalyst **2**, and to a lesser extent than catalyst **1**.

Notably, for what concerns phosphine-free catalysts **5–8**, differently from the RCM of **9** and **11** where all the catalysts gave very high reaction rates as well as fast initiation, in the RCM of **13** *N*-*o*-tolyl catalysts **5** and **6** retained fast initiation rates, whereas **7** and **8** initiated slowly (Fig. 4B). Therefore, while **5** and **6** converted almost quantitatively **17** within 60 min, **7** and **8** reached 86% and 78% conversion, respectively, completing cyclization within 7 h. The slowest initiation makes **8** the less performing among the herein reported catalysts in the RCM of hindered olefins. The reactivity trend observed in the RCM of malonate derivative **17** was not respected in the less difficult ring-closure of tosyl derivative **19**, where all catalysts gave nearly full conversions in 30 min (Fig. 4D).

 

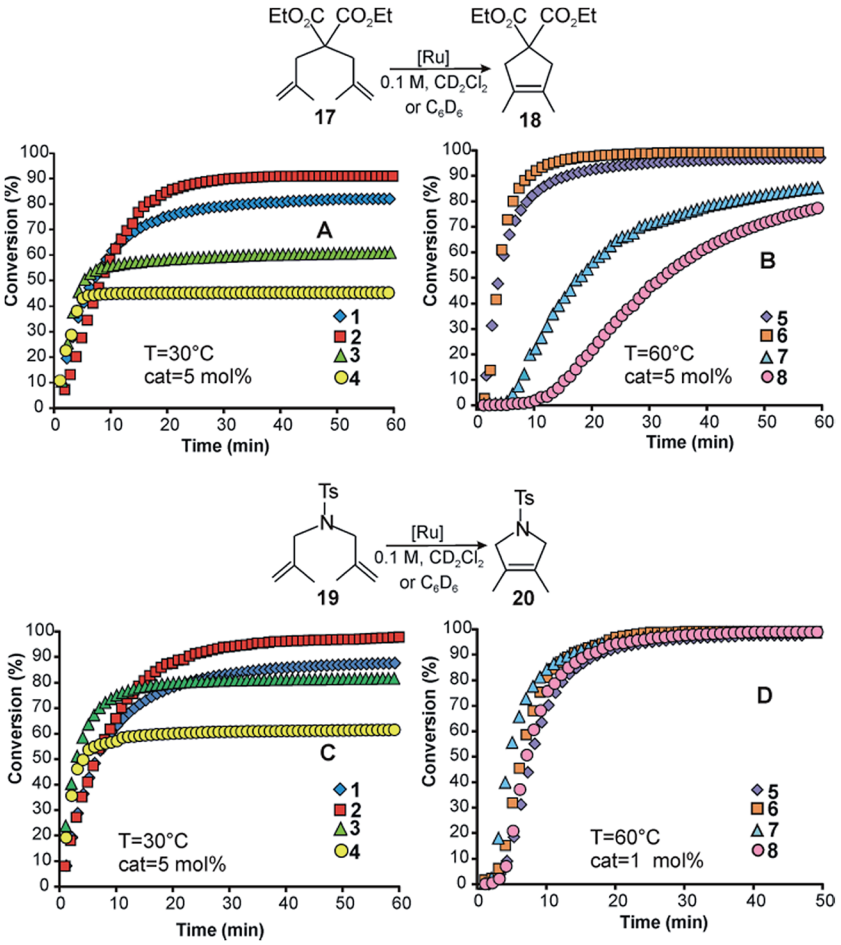


Fig. 4 Kinetic plots of the RCM of **17** and **19**.

### Steric and electronic properties of NHCs

In order to find correlations between the structural features of NHCs **L1–L4** and catalytic behaviors of related ruthenium complexes **1–8**, the steric and electronic properties of the carbenes were assessed by using various metrics.[11] To quantify experimentally the steric and electronic parameters of NHC ligands, rhodium(I) derivatives of general formula [RhCl(COD)(NHC)] (COD = 1,5-cyclooctadiene) and [RhCl(CO)$_2$(NHC)] are commonly employed as valuable probes, thanks to the their ease of preparation and high stability.[3i,12] For these purposes, two series of new rhodium complexes, consisting of cyclooctadiene derivatives **21–24** and bis(carbonyl) derivatives **25–28** incorporating the NHCs of interest, were synthesized (Scheme 2).

Reaction of dihydroimidazolium salts of NHCs **L1–L4** with KHMDS in toluene at room temperature and subsequent treatment with [RhCl(COD)]$_2$ afforded, after purification by column chromatography, the desired Rh complexes **21–24** as yellow, air stable solids in good yields (67–83%). Rhodium carbonyl complexes **25–28** were then obtained in quantitative yields by bubbling CO in $CH_2Cl_2$ solutions of **21–24** (Scheme 2). All complexes were fully characterized by one- and two dimensional $^1$H and $^{13}$C NMR techniques, and, for rhodium

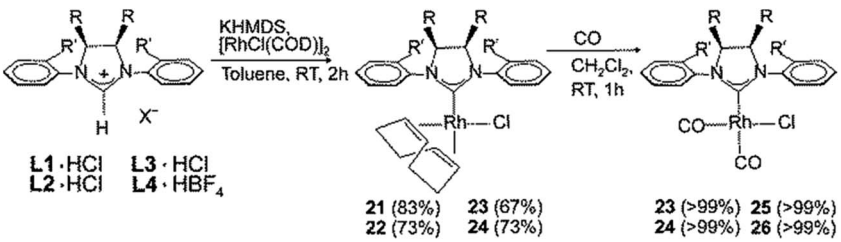


Scheme 2 Synthesis of Rh complexes **21–24** and **25–28**.

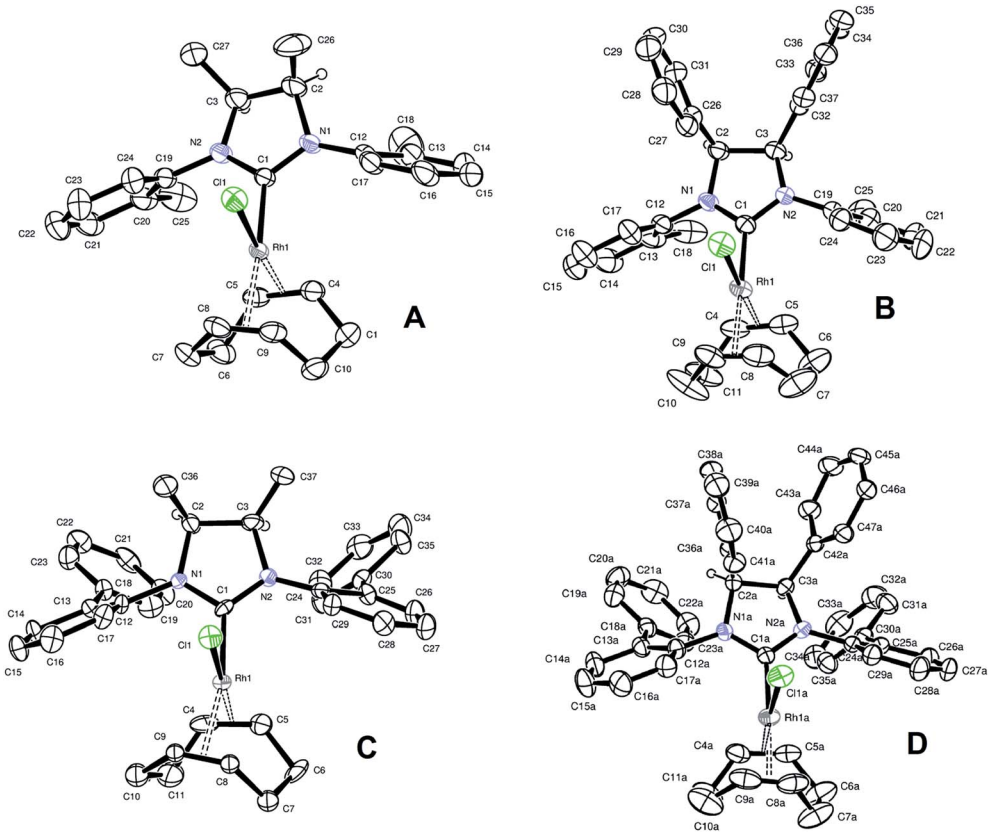


Fig. 5 ORTEP[8] view of complexes **21** (A), **22** (B), **23** (C) and **24** (D) with the thermal ellipsoids at 30% probability. The H atoms, excluded those linked to C2 and C3 carbons of the NHC ring, have been omitted for sake of clarity.

cyclooctadiene derivatives **21–24**, single crystals suitable for X-ray structure analysis were independently obtained.[13]

The resulting molecular structures are depicted in Fig. 5.

In all the four **21–24** compounds the Rh center adopts a square planar coordination geometry. The Cl1 and C1(NHC) atoms are *trans* oriented to the C=C π systems of the COD alkene molecule.

In all complexes the distances of the Rh center to the centroids at the COD alkene bonds are longer for those *trans* to NHC [2.10 Å, on average] than for those *trans* to Cl1 atom [1.98 Å, on average]. This can be ascribed to the greater *trans* influence of NHC moiety.

Furthermore, the square coordination planes are almost perpendicular to NHC rings making angles of 87.61(8), 88.13(8) and 89.6(1)° for complexes **21–23**, respectively, and 87.8(1) and 85.6(1)° for molecules A and B of compound **24**. The phenyl substituted rings linked to the NHC nitrogens, N1 and N2, are twisted with respect to the NHC ring. These conformations are

Table 1 Selected data for the characterization of NHCs **L1–L4** in metal complexes used herein

| | **L1** | **L2** | **L3** | **L4** |
|---|---|---|---|---|
| % $V_{Bur}$ from **21–24**[a] | 33.4 | 34.0 | 34.8 | 34.8 ± 0.1[b] |
| % $V_{Bur}$ from **5–8**[c] | 32.3 | 33.1 | 33.9 | 34.7 |
| $^1$H NMR chemical shift in **21–24**[d] | 4.38 ppm | 4.70 ppm | 4.87 ppm | 5.06 ppm |
| $\nu_{av}$(CO) for **25–28**[e] | 2037.5 cm$^{-1}$ | 2039.5 cm$^{-1}$ | 2039.0 cm$^{-1}$ | 2042.0 cm$^{-1}$ |
| TEP from **25–28**[f] | 2050.2 cm$^{-1}$ | 2051.8 cm$^{-1}$ | 2051.4 cm$^{-1}$ | 2053.8 cm$^{-1}$ |
| $\Delta E_{1/2}$ for **1–4**[g] | 0.467 V | 0.583 V | 0.574 V | 0.671 V |
| $\Delta E_{1/2}$ for **5–8**[g] | 0.897 V | 0.956 V | 0.967 V | 1.05 V |
| BDE for **25–28**[h] | 55.2 kcal mol$^{-1}$ | 54.8 kcal mol$^{-1}$ | 52.8 kcal mol$^{-1}$ | 52.2 kcal mol$^{-1}$ |

[a] Obtained from crystallographic data. [b] Average of the two independent structures. [c] Obtained from DFT optimized structures. [d] δ (=C*H*) of the olefin *trans* to the NHC registered in $CD_2Cl_2$. [e] Carbonyl stretching frequencies determined using IR spectroscopy for complexes in $CH_2Cl_2$ solutions. [f] Calculated using the equation TEP = 0.8001$\nu_{av}$(CO) + 420.0 cm$^{-1}$. [g] Redox potentials determined using cyclic voltammetry in $CH_2Cl_2$ under nitrogen; 0.1 M $NH_4PF_6$ as supporting electrolyte; internal reference octamethylferrocene; scan rate 100 mV s$^{-1}$. [h] Determined by DFT calculations.

 

probably related to short H···C(phenyl ring) interactions, of about 2.70 Å such as: H4···C12 and H5···C19, in compounds **21** and **22**, as well asH4···C12 and H5···24 in compounds **23** and **24**. All the other structural parameters are in good agreement with those observed for other similar complexes.

Evaluation of the steric bulkiness of the NHCs **L1–L4** of complexes **21–24** was made by calculating the percentage of buried volume (% $V_{Bur}$) of each NHC ligand from the crystal data of the corresponding Rh complex *via* the computational tool Samb*V*ca2 developed by Cavallo.[14] The % $V_{Bur}$ values are reported in Table 1. Although very close, these values well correlate with the size of the substituents within the NHC framework. Moving from methyl to phenyl substituents, steric bulk is higher when the more encumbered phenyl groups are located on the *ortho* positions of the *N*-phenyl rings rather than on the backbone. The most significant steric variation in the examined NHCs is observed changing from all methyl (**L1**) to all phenyl substituents (**L4**). The same trend was found for the % $V_{Bur}$ values extracted from the Density Functional Theory (DFT) optimized geometries of ruthenium complexes **5–8**.[15]

The steric impact of the different NHCs was investigated at the molecular level analyzing the topographic steric maps calculated for both Rh complexes **21–24** and Ru complexes **5–8** (Fig. 6). The steric contour maps for rhodium complexes reported in Fig. 5 (left) show that the steric hindrance of the NHC ligands is located in the lower part of the map (on the left and on the right) where the more intense yellow area for **23** and **24** corresponds to an increased bent of the *N*-phenyl groups due to the growth of the *ortho* substituents. The nature of the distribution of the NHC ligands **L1–L4** around the metal center in the topographic steric maps of **5–8** with analogous ligands (Fig. 6, right) reflects the adaptability of NHCs to the changed geometry of Ru complexes with respect to Rh compounds. Indeed, differently from NHC–Rh complexes, an additional asymmetry has to be considered for **5–8**. NHC–Ru carbene bonds are not collinear with *z*-axis depicted in the topographic steric maps, as already shown by Cavallo *et al.*,[14,16] leading to an increase of ligand steric hindrance illustrated by orange contour line on the right low quadrant.

To assess the electronic properties of NHCs **L1–L4**, in analogy with the approach presented by Bielawski,[17] we investigated rhodium complexes **21–28** using spectroscopic techniques. The series of rhodium derivatives presenting a cyclooctadiene ligand in *trans* position to the NHCs **L1–L4** (**21–24**) was studied by $^{1}$H NMR spectroscopy. Dependently from electron density on the metal, coordinated *trans* double bond of the olefin can act as a classical two-electron donor maintaining a significant degree of double bond, or adopt metallocyclopropane character as a consequence of metal-to-olefin π-backbonding. The capacity of NHCs to participate in π-backbonding interactions can be thus estimated by the chemical shifts of the olefin protons *trans* to the NHC ligand.[18] The values observed for the diagnostic olefinic protons of **21–24** are summarized in Table 1. The nature of the substitution pattern of **L1–L4** seems to exert a profound effect on the electron donor ability of the NHC ligand. The most significant difference (0.68 ppm) was observed for complexes **21** and **24**

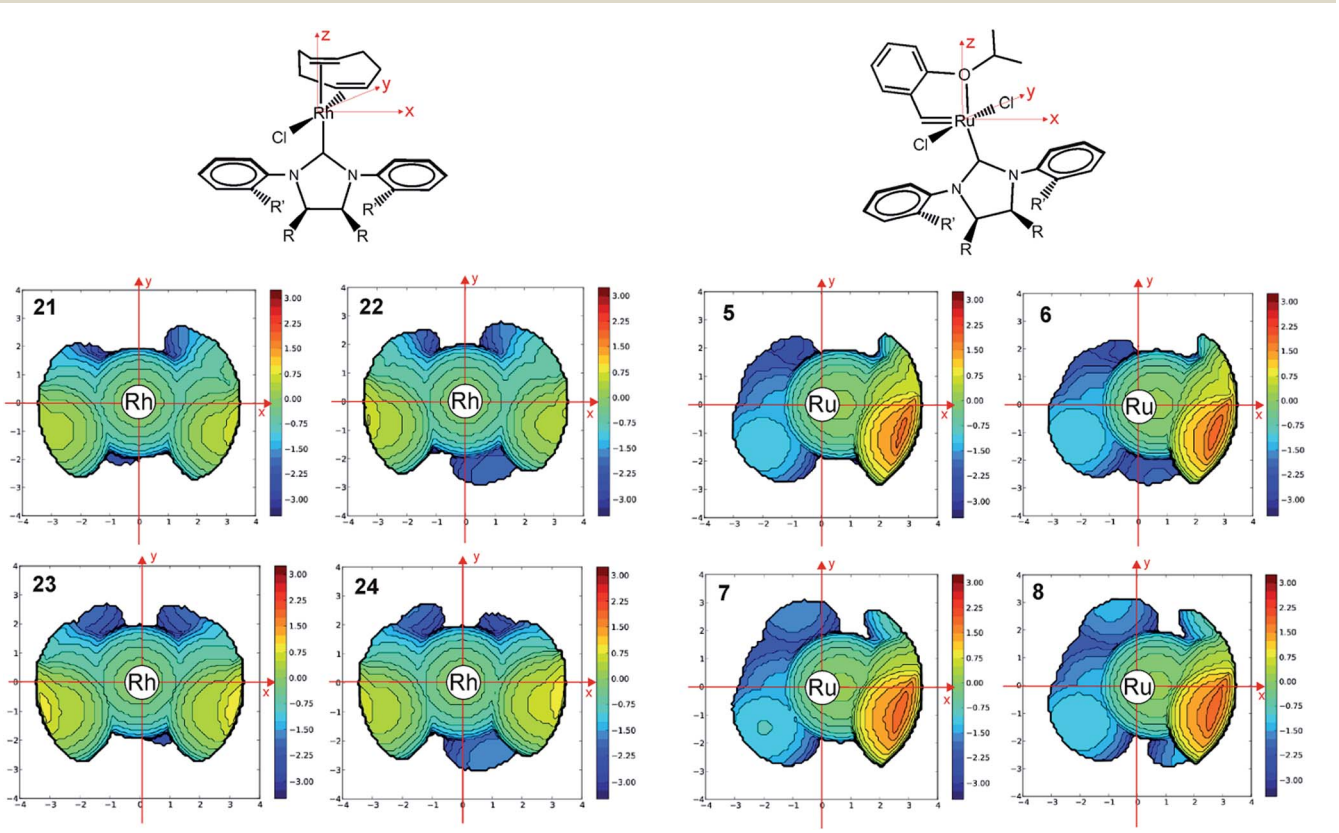


Fig. 6 Topographic steric maps of **21–24** (left) and **5–8** (right). The iso-contour curves are in Å.

bearing all methyl and all phenyl substituents, respectively, and could be interpreted as a consequence of the different group electronegativities of methyl and phenyl groups.[19] A much less marked difference for complexes **22** and **23** characterized by mixed methyl–phenyl substituents on the NHC ring (0.17 ppm) was registered, suggesting a negligible effect of the relative disposition of methyl and phenyl groups within the NHC ring on the resulting NHC electron donicity.

As for rhodium derivatives **25–28** containing a CO ligand in *trans* to the NHC, π-back-bonding contribution were assessed by IR spectroscopy. IR spectra for **25–28** were recorded in $CH_2Cl_2$ and the average stretching frequencies of the carbonyl ligands $\nu_{av}$(CO) were listed in Table 1.

The Tolman electronic parameters (TEPs)[20] of the NHCs **L1–L4** were then estimated from the average stretching vibration wavenumbers (Table 1) using the linear regression proposed by Dröge and Glorius.[21] The values obtained suggest a more electron-donating nature for the NHC **L1**, bearing methyl groups as substituents on both the backbone and the *N*-phenyl rings, with respect to the analogue NHC **L4** with all phenyl substituents (2050.2 $cm^{-1}$ for **L1** *vs.* 2053.8 for **L4**). This finding is consistent with previous results and can be explained considering the methyl substituents as better donors than phenyl groups. The hybrid substitution patterns represented by NHCs **L2** and **L3** showed TEP values nearly identical, suggesting that electronic contribution of backbone substituents is in turn compensated by an almost equal and opposite contribution of substituents on the *N*-aryl groups.

To gain more information on the electronic situation at the metal center, we decided to supplement measured TEP data for **L1–L4** with electrochemical studies[22] of Ru complexes **1–8**. Indeed, while TEP is a measurement of the ability of a metal center to donate electron density into the π* orbital of a CO ligand, the redox potential of a metal center should provide a measure of the electronic density at the metal center. The Ru(II)/Ru(III) redox potentials for complexes **1–8** were established by cyclic voltammetry and presented in Table 1. A very similar trend was observed for both the series of Grubbs' and Hoveyda–Grubbs' second generation catalysts, with an anodic shift of about +0.400 V changing from phosphine-containing catalysts **1–4** to the corresponding oxygen-chelated complexes **5–8**, as already reported by Plenio in an analogous comparative study.[23]

The electron donating properties of the NHCs **L1–L4**, determined studying the electrochemistry of the related ruthenium complexes, were found to be in very good agreement with those determined through IR spectroscopy of the corresponding rhodium carbonyl complexes. The difference between the most and the least electron-donating NHC, **L1** and **L4**, respectively, is 0.204 V for the series of Grubbs' second generation catalysts, and 0.153 V for the series of Hoveyda' second generation catalysts. Within the two classes of catalysts, the replacement of a methyl group of **L1** by a phenyl group to give **L2** or **L3** leads to anodic shifts of the Ru(II)/Ru(III) redox potentials (59–116 mV), indicating a lower electron density at the metal center; on the other hand, the replacement of a phenyl group of **L4** by a methyl group to provide **L2** or **L3** implies a higher electron density at the metal center, as underlined by cathodic shifts of the redox potentials (83–97 mV). Very small change in redox potential (9–11 mV) of complexes characterized by NHCs **L2** and **L3** with mixed methyl and phenyl substituents, alternatively on the backbone or at the *ortho* positions of *N*-phenyl groups, confirming that the relative disposition of these substituents on the NHC ring is not relevant in terms of resulting NHC electronic properties. This finding provides a further evidence of the combined effect of backbone substitution and *N*-aryl substitution in determining electronic properties of the NHC ligand. In particular, with regard to the *N*-aryl substituents, we can consider that interaction between electron active *ortho*-groups of *N*-aryl substituents and metal center operates "through space" *via* donation from the C*ipso* atom of the *N*-substituent, as described by Plenio and Cavallo for NHC ruthenium complexes characterized by *para*-groups on the *N*-aryl substituents.[24] It is worthy to underline, moreover, that the presence of *ortho*-substituents influences at the same time both steric and electronic properties of the system.

As a further characterization, bond-dissociation energies (BDE) for NHCs **L1–L4** from **25–28** were evaluated by DFT calculations (see ESI for computational details†) and were reported in Table 1.[25]

The BDE are mainly affected by two factors: the electron donation of the backbone substituents and the different dimension of *ortho N*-aryl substituents. Electron donation of the backbone substituents seems to play a minor role: the BDE differences between **L1** and **L2** and between **L3** and **L4** are 0.4 and 0.6 kcal $mol^{-1}$, respectively, with backbone methyl substituted **L1** and **L3** presenting higher BDE with respect to the corresponding phenyl substituted **L2** and **L4**. By modeling simplified complexes with NHCs bearing *N*-methyl substituents, similar BDE energy gap (0.8 kcal $mol^{-1}$) was also found between methyl and phenyl backbone substituted NHCs. Higher energy gaps can be observed comparing NHCs with different *ortho N*-aryl substituents (2.4 kcal $mol^{-1}$ between **L1** and **L3**, 2.6 kcal $mol^{-1}$ between **L2** and **L4**). We believe that these differences can be mainly ascribed to the steric hindrance of the *ortho N*-aryl substituents, that involves a major repulsion with the other ligands and that causes the main energy gaps among these complexes. As a consequence, together with the % $V_{Bur}$ and the steric maps, also the BDE can be read as another measure of the NHC steric hindrance.

In light of the above results, catalytic outcomes of previously described RCM reactions promoted by ruthenium complexes **1–8** turned out to be principally dominated by steric factors. As for phosphine-containing catalysts **1–4**, the best performances in the easy ring closures of substrates **9** and **11** were registered with **3** and **4**, presenting the most encumbered NHCs (**L3** and **L4**), whereas no correlation between the electron donor abilities of the carbenes and the observed reactivity trend was found. Moreover, catalysts **1** and **2**, possessing very similar steric bulkiness, behave likewise although electronic properties of **L1** and **L2** are quite different. Therefore, the size of *N*-substituents of the NHC ligands (*o*-biphenyl *vs. o*-tolyl) seems to be the key factor in determining catalyst efficiency. It is worth to underline that the steric bulk of *N*-substituents of the NHC ligands in

 

monophosphine ruthenium complexes has been reported to have a great influence on the catalytic activities of the corresponding complexes, favoring the dissociation of the phosphine ligand and facilitating the formation of the 14-electron active species.[26] However, faster initiation does not improve reaction rates but, on the contrary, is related to a faster decomposition, caused by attack of free phosphine to propagating Ru–methylidene species.[4] This drawback becomes more evident with the increase of steric hindrance of RCM substrates. In fact, in the RCM of **11** and **17**, **3** is confirmed as the best performing catalyst, whereas the efficiency of **4** worsens significantly, and in the most sterically demanding RCM of **13** and **19**, both **3** and **4** were surpassed by less encumbered catalysts **1** and **2**. Between **3** and **4** possessing NHCs with roughly the same steric hindrance the highest conversions were constantly reached with catalyst **3**. This finding could be a consequence of the more electron donating character of NHC **L3**, which could better stabilize the 14-electron active species and lead to better catalytic efficiency. Nevertheless, steric factors affecting the propagation step of the reaction cannot be excluded.

The slightly different behavior of **1** and **2** appreciable in the RCM of more hindered diolefins **13** and **19** may be explained considering again steric factors. Indeed, as already reported,[3e] catalyst **1** exists as a mixture of conformers with *syn* and *anti* oriented *N*-*o*-tolyl groups, the latter offering a slightly more crowded reactive pocket to accommodate encumbered substrates.

The above considerations about correlations between steric and electronic properties of NHCs **L1–L4** and catalyst behavior cannot be easily extended to the series of phosphine free catalysts **5–8**. In this case, the absence of decomposition pathways of the active species ensures high efficiency for all the catalysts and the most significant result is related to the slow initiation rate observed for catalysts **7** and **8** in the RCM of **13**. This finding contrasts sharply with the behavior shown by the analogous phosphine-containing catalysts **3** and **4** in the same RCM transformation, where actually they displayed high initiation rates, even if followed by a rapid decomposition, and may be ascribed to the different initiation mechanism for the two families of catalysts. The different behavior of **5–6** and **7–8** registered only in the RCM of the most challenging malonate derivative **13** would suggest that the nature of the substrate plays an important role during the initial step of the reaction.

## DFT calculations

To clarify this issue, theoretical studies were undertaken. It should be first noted that the initiation mechanism in the presence of Hoveyda-type catalysts is still under discussion.[27] Grubbs showed that entropy of activation is negative, implying an interchange or an associative mechanism,[28] whereas later studies by Plenio suggested a simultaneous competition between a dissociative and an interchange.[29] Computational work conducted by Solans-Monfort concluded that, while associative mechanism appeared clearly unfavored, neither the dissociative nor the interchange mechanism can be excluded as possible initiation mechanisms.[30]

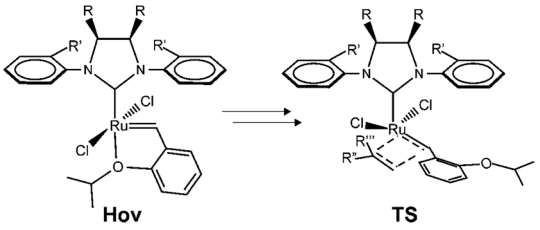


Scheme 3 Hoveyda-type catalysts and TS previous MCB.

In the light of computational studies conducted by Hillier and Percy[31] where, for substituted olefins as propene, highest energy barrier during the initiation was identified as the transition state (TS) leading to the formation of metallacyclobutane (MCB), we performed DFT calculations on the barriers for the formation of metallacyclobutane in case of substrates **9** (or **13**)[32] and **17** [33] with catalysts **5–8**, by locating the geometries and energies of starting Hoveyda-type catalysts and the TS previous MCB (Scheme 3).

Due to ligand symmetry, four possible TS can be located for each catalyst depending on the orientation of the substrate and of the benzylidene alkoxy moiety. In Fig. 7, TS free energy barriers, calculated as energy difference between the TS and the corresponding Hoveyda catalyst (Scheme 3), for low hindered substrate **9** (or **13**) in the presence of *o*-methyl *N*-aryl catalysts **5** and **6** are reported. The TS species are shown in quadrant

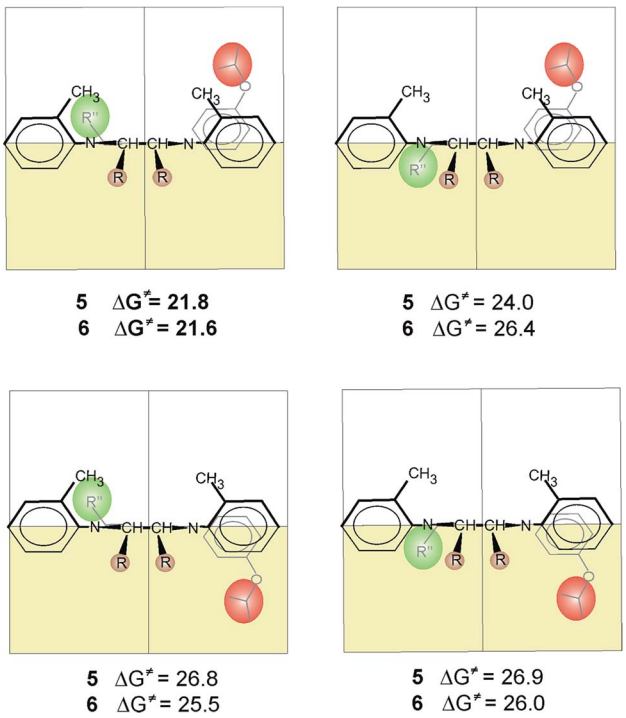


Fig. 7 Transition state free energies (TS in Scheme 3) involving low hindered substrate **9** (or **13**)[32] in the presence Hoveyda-type catalysts **5** and **6**. The TS species are shown in quadrant representation, viewed along the NHC–Ru bond. Yellow quadrants represent hindered space due to the bent-down *N*-phenyl groups. Free energies are in kcal $mol^{-1}$.

representation, viewed along the NHC–Ru bond. Yellow quadrants represent hindered space due to the bent-down *N*-phenyl groups.

Indeed, is not surprising that the lowest energy TS geometries involve substrate and alkoxy benzylidene moiety oriented toward the less encumbered catalyst side for both **5** and **6**. Lowest TS free energy barriers are also very similar for the two catalysts, being 21.8 and 21.6 kcal mol$^{-1}$ for **5** and **6**, respectively.

As for *o*-phenyl *N*-aryl catalysts 7 and **8** in the RCM of **9** and **13**, the space occupancy of the ligand is quite different, as already highlight with steric maps in previous section. Corresponding TS free energies are reported in Fig. 8 and TS species are shown in quadrant representation as well. Yellow quadrants always represent hindered space due to the bent-down *N*-phenyl groups, whereas orange quadrants represent hindered space due to the *o*-phenyl *N*-aryl groups. The *o*-phenyl substituents balance the hindrance on the two sides of the catalysts producing as primary effect the increasing of energy barriers, which are, as secondary effect, flattened with respect to the possible substrate and alkoxy benzylidene moiety orientations. Lowest barriers where located at 26.9 and 26.6 kcal mol$^{-1}$ for 7 and **8**, respectively.

Finally, TS free energy barriers were located for all catalysts **5–8** in case of challenging substrate **17**. Only lowest barriers have been reported for **5–8** in Fig. 9, in quadrants representation. Corresponding geometries are shown in Fig. 10 (**TS-5**, **TS-6**, **TS-7**, **TS-8**). TS energies climb up to 30–35 kcal mol$^{-1}$, due to substrate hindrance. Catalyst **6** gives the lowest barrier (29.9 kcal mol$^{-1}$), whereas *N*-*o*-biphenyl substituted catalysts **7–8** showed the highest barriers (35.8 and 36.1 kcal mol$^{-1}$ respectively).

Computational results are able to rationalize the experimental kinetic data reported above for catalysts **5–8**. Indeed, the induction period observed for catalysts 7 and **8** in the RCM of hindered substrates would be generated by high TS barriers for the formation of the MCB in the initiation step. The same induction period is not visible for catalyst **5** and **6** that give significantly lower barriers, neither for catalysts 7 and **8** in the RCM of substrates **9** and **13** for the same reason.

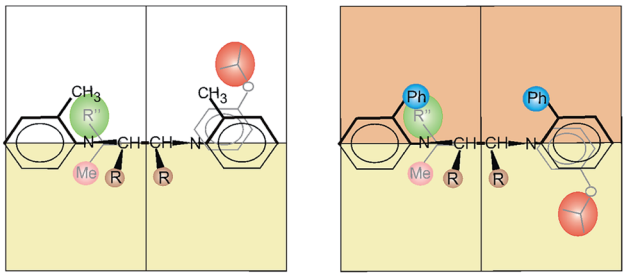


Fig. 9 Lowest transition state free energies (TS in Scheme 3) involving highly hindered substrate **17** [33] in the presence Hoveyda-type catalysts **5–8**. The TS species are shown in quadrant representation, viewed along the NHC–Ru bond. Yellow quadrants represent hindered space due to the bent-down *N*-phenyl groups, whereas orange quadrants represent hindered space due to the *o*-phenyl substituents. Free energies are in kcal mol$^{-1}$.

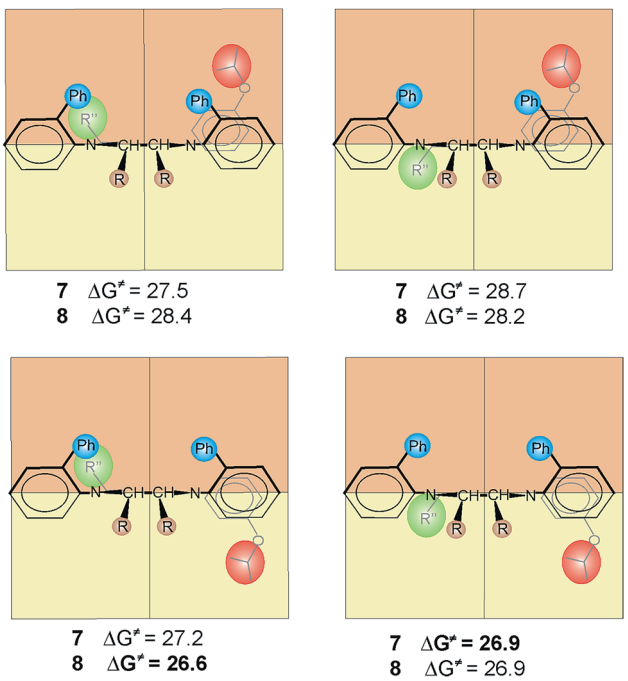


Fig. 8 Transition state free energies (TS in Scheme 3) involving low hindered substrate **9** (or **13**)[32] in the presence Hoveyda-type catalysts 7 and **8**. The TS species are shown in quadrant representation, viewed along the NHC–Ru bond. Yellow quadrants represent hindered space due to the bent-down *N*-phenyl groups, whereas orange quadrants represent hindered space due to the *o*-phenyl substituents. Free energies are in kcal mol$^{-1}$.

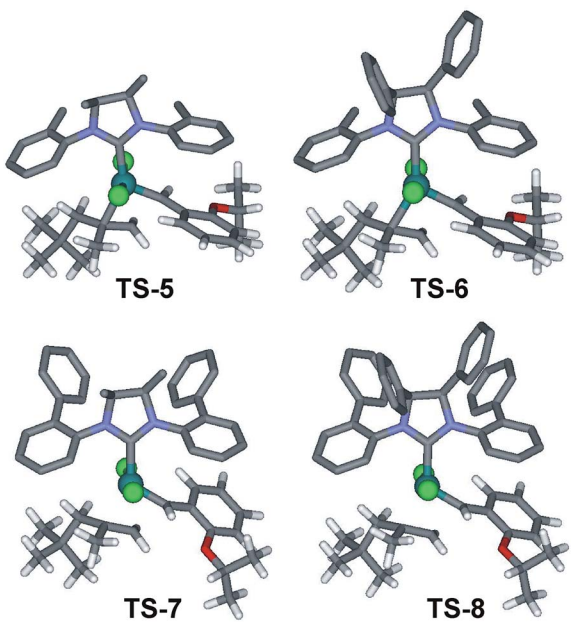


Fig. 10 Lowest free energy transition state geometries (also reported in quadrant representation in Fig. 9) involving highly hindered substrate **17**[33] in the presence Hoveyda catalysts **5–8**.

## Conclusions

In the present study, we have reported the synthesis and characterization of two new Grubbs and Hoveyda–Grubbs type complexes bearing NHCs with *N*-*o*-biphenyl substituents and, alternately, *syn* methyl (**3**, **7**) or *syn* phenyl groups (**4**, **8**) on the backbone. Their catalytic behaviors were investigated in model RCM reactions and compared to those of already known related complexes possessing *N*-*o*-tolyl groups. The introduction of more encumbered *ortho* phenyl instead of *o*-methyl groups led to quite conflicting results. Indeed, while with catalyst **3**, incorporating *syn* methyl groups on the backbone, an outstanding improvement of reaction rates was observed in the easiest RCM reactions forming a di- or trisubstituted cycloolefin, with catalyst **4**, having phenyl groups on the backbone, the same behaviour was found only in the formation of disubstituted cycloolefins. It is worth to underline that catalyst **3** has been identified as the most efficient system known to date in this class of RCM reactions. With the increase of the steric hindrance of the RCM substrates, the presence of *N*-*o*-biphenyl substituents revealed to be not beneficial for the successful accomplishment of the reactions. As for the series of Hoveyda-type complexes, a similar trend in catalytic behavior may be noticed, even if the reactivity differences are definitely attenuated. Interestingly, the RCM of malonate derivative **17** promoted by *N*-*o*-biphenyl catalysts **7** and **8** displayed a marked induction period than in the presence of corresponding *N*-*o*-tolyl catalysts **5** and **6**. To establish correlation between catalytic outcomes and structural features of NHCs involved (**L1–L4**), a detailed characterization of the steric and electronic parameters of these carbenes was performed using different metrics, based also on the employment of new rhodium derivatives **21–28**. The steric demand of **L1–L4** was quantified as % $V_{Bur}$ using X-ray analysis of rhodium cyclooctadiene complexes **21–24** and DFT optimized geometries of ruthenium isopropoxybenzylidene complexes **5–8**. Also the BDE evaluated from rhodium carbonyl complexes **25–28** were employed as a measure of the steric hindrance of **L1–L4**. The most significant steric difference in the examined NHCs is between **L1** and **L4**, containing all methyl and all phenyl substituents, respectively. The electronic properties of **L1–L4** were quantified employing the carbonyl IR stretching frequencies of rhodium complexes **25–28** (TEP method) and through electrochemical studies on ruthenium complexes **1–8**. **L1** and **L4** were found to be the most and the less electron donating NHC, respectively, while **L3** and **L4**, characterized by opposite arrangement of methyl and phenyl substituents within the NHC ligand, showed nearly the same donor ability, indicating a negligible role of their relative disposition.

Therefore, to summarize, we have illustrated that the systematic variation of substituents on the NHC backbone and on the *ortho* positions of the *N*-aryl substituents (methyl and/or phenyl) allowed the fine-tuning of the stereoelectronic properties of the corresponding ligands. Although electronic effects deriving from the different substitution within the NHC ligand proved to be important, no correlations with catalytic results emerged. On the other hand, small differences in the steric environment provided by the NHC around the metal seems to cause a significantly different catalytic behavior. The predominance of steric on electronic effects was also found to be responsible for the induction period observed for catalysts **7** and **8** in the RCM of hindered substrates, as suggested by DFT calculations. The search for the right balance between steric hindrance of NHC backbone substituents and *N*-aryl groups is therefore crucial in the development of tailor-made RCM catalysts. More in general, fully understanding of sterics and electronics of NHCs **L1–L4** represents an important advancement for their application not only in organometallic catalysis, but also in organocatalysis.

## Acknowledgements

The authors thank Dr Patrizia Iannece, Dr Ivano Immediata, Patrizia Oliva for technical assistance. Financial support from the Ministero dell'Università e della Ricerca Scientifica e Tecnologica is gratefully acknowledged.

## References

1 (*a*) R. H. Grubbs, *Handbook of Metathesis*, Wiley-VCH, Weinheim, Germany, 2003, vol. 1–3; (*b*) S. J. Connon and S. Blechert, in *Ruthenium Catalysts and Fine Chemistry*, ed. P. H. Dixneufand C. Bruneau, Springer, Heidelberg, Germany, 2004, vol. 11, p. 93; (*c*) A. Fürstner, *Angew. Chem.*, 2000, **112**, 3140; *Angew. Chem., Int. Ed.*, 2000, **39**, 3012; (*d*) A. H. Hoveyda and A. R. Zhugralin, *Nature*, 2007, **450**, 243; (*e*) P. H. Deshmuhk and S. Blechert, *Dalton Trans.*, 2007, 2479; (*f*) D. Astruc, *New J. Chem.*, 2005, **29**, 42; (*g*) A. M. Lozano-Vila, S. Monsaert, A. Bajek and F. Verpoort, *Chem. Rev.*, 2010, **110**, 4865; (*h*) *Olefin Metathesis Theory and Practice*, ed. K. Grela, J. Wiley & Sons, Hoboken, NJ, 2014.

2 (*a*) G. C. Vougioukalakis and R. H. Grubbs, *Chem. Rev.*, 2010, **110**, 1746; (*b*) C. Samojlowicz, M. Bieniek and K. Grela, *Chem. Rev.*, 2009, **109**, 3708; (*c*) M. Bieniek, A. Michrowska, D. L. Usanov and K. Grela, *Chem.–Eur. J.*, 2008, **14**, 806; (*d*) V. Paradiso, C. Costabile and F. Grisi, *Molecules*, 2016, **21**, 117.

3 (*a*) I. C. Stewart, T. Ung, A. A. Pletnev, J. M. Berlin, R. H. Grubbs and Y. Schrodi, *Org. Lett.*, 2007, **9**, 1589; (*b*) J. M. Berlin, K. Campbell, T. Ritter, T. W. Funk, A. Chlenov and R. H. Grubbs, *Org. Lett.*, 2007, **9**, 1339; (*c*) C. K. Chung and R. H. Grubbs, *Org. Lett.*, 2008, **10**, 2693; (*d*) K. M. Kuhn, J.-B. Bourg, C. K. Chung, S. C. Virgil and R. H. Grubbs, *J. Am. Chem. Soc.*, 2009, **131**, 5313; (*e*) F. Grisi, A. Mariconda, C. Costabile, V. Bertolasi and P. Longo, *Organometallics*, 2009, **28**, 4988; (*f*) C. Costabile, A. Mariconda, L. Cavallo, P. Longo, V. Bertolasi, F. Ragone and F. Grisi, *Chem.–Eur. J.*, 2011, **17**, 8618; (*g*) A. Perfetto, C. Costabile, P. Longo, V. Bertolasi and F. Grisi, *Chem.–Eur. J.*, 2013, **19**, 10492; (*h*) A. Perfetto, C. Costabile, P. Longo and F. Grisi, *Organometallics*, 2014, **33**, 2747; (*i*) Y. Borguet, G. Zaragoza, A. Demonceau and L. Delaude, *Dalton Trans.*, 2015, **44**, 9744.

4 S. H. Hong, A. Chlenov, M. W. Day and R. H. Grubbs, *Angew. Chem., Int. Ed.*, 2007, **46**, 5148.

5 S. Y. M. Chooi, P.-h. Leung, S.-c. Ng, G. H. Quek and K. Y. Sim, *Tetrahedron: Asymmetry*, 1991, **2**, 981.
6 The synthesis of the analogous chloride salt was also attempted. No formation of the desired product was observed.
7 (*a*) The low yield obtained for complex **3** was ascribed to a partial decomposition occurring during the step of purification, very likely related to the rather low stability of the complex in solution; (*b*) Complex **3** decompose in both $CD_2Cl_2$ and $C_6D_6$ solution within 24 h, therefore its NMR characterization was limited to $^1H$ and $^{31}P$ NMR experiments.
8 M. N. Burnett and C. K. Johnson, *ORTEP III, Report ORNL-6895*, Oak Ridge National Laboratory, Oak Ridge, TN, 1996.
9 (*a*) M. B. Dinger and J. C. Mol, *Adv. Synth. Catal.*, 2002, **344**, 671; (*b*) T. Ritter, A. Hejl, A. G. Wenzel, T. W. Funk and R. H. Grubbs, *Organometallics*, 2006, **25**, 5740.
10 It should be noted that the very fast RCM reactions of *N*-tosyl derivatives **11**, **15** and **19** promoted by catalysts **5–8** were performed at a lower catalyst loading than the corresponding with malonate derivatives to better appreciate differences in catalyst behaviour.
11 (*a*) L. Falivene, A. Poater and L. Cavallo, in *N-Heterocyclic Carbenes: Effective Tools for Organometallic Synthesis*, ed. S. P. Nolan, Wiley-VCH, 2014; (*b*) D. J. Nelson and S. P. Nolan, *Chem. Soc. Rev.*, 2013, **42**, 6723.
12 Selected examples: (*a*) S. Wolf and H. Plenio, *J. Organomet. Chem.*, 2009, **694**, 1487; (*b*) M. Iglesias, D. J. Beetstra, B. Kariuki, K. J. Cavell, A. Dervisi and I. A. Fallis, *Eur. J. Inorg. Chem.*, 2009, **13**, 1913; (*c*) R. Savka and H. Plenio, *Eur. J. Inorg. Chem.*, 2014, 6246; (*d*) C. Mejuto, G. Guisado-Barrios and E. Peris, *Organometallics*, 2014, **33**, 3205; (*e*) V. Paradiso, V. Bertolasi, C. Costabile and F. Grisi, *Dalton Trans.*, 2016, **45**, 561; (*f*) R. Savka, M. Bergmann, Y. Kanai, S. Foro and H. Plenio, *Chem.–Eur. J.*, 2016, **22**, 9667.
13 Single crystals of **21–24** were obtained by slow evaporation of a $CH_2Cl_2$/pentane 2 : 1 mixture. Any attempts to obtain crystals for rhodium carbonyl complexes **25–28** failed.
14 L. Falivene, R. Credendino, A. Poater, A. Petta, L. Serra, R. Oliva, V. Scarano and L. Cavallo, *Organometallics*, 2016, **35**, 2286. The default processing parameters of *SambVca* 2.0 web application were kept unchanged.
15 Since no X-ray structure was available for complex **8**, DFT optimized structures of **5–8** were used for the % $V_{Bur}$ calculation % $V_{Bur}$ values determined by DFT are in good agreement with % $V_{Bur}$ from X-ray structures of **5–7**.
16 F. Ragone, A. Poater and L. Cavallo, *J. Am. Chem. Soc.*, 2010, **132**, 4249.
17 (*a*) D. M. Khramov, V. M. Lynch and C. W. Bielawski, *Organometallics*, 2007, **26**, 6042; (*b*) D. M. Khramov, E. L. Rosen, J. A. V. Er, P. D. Vu, V. M. Lynch and C. W. Bielawski, *Tetrahedron*, 2008, **64**, 6853.
18 Only few data on $^1H$ NMR chemical shift measurements used to evaluate electronic properties of NHCs in [RhCl(COD)(NHC)] complexes are available in the literature (see ref. 17), thus conclusions drawn from this method could be questionable and need to be confirmed by other metrics.
19 Group electronegativities: $CH_3$ 2.3, Ph 3.0, see: (*a*) P. R. Wells, *Prog. Phys. Org. Chem.*, 1968, **6**, 111; (*b*) E. V. Anslyn and D. A. Dougherty, *Modern Physical Organic Chemistry*, University Science Books, Sausalito, CA, 2006, p. 16.
20 C. A. Tolman, *Chem. Rev.*, 1977, **77**, 313.
21 T. Dröge and F. Glorius, *Angew. Chem., Int. Ed.*, 2010, **49**, 6940.
22 (*a*) A. B. P. Lever, *Inorg. Chem.*, 1990, **29**, 1271; (*b*) A. B. P. Lever, *Inorg. Chem.*, 1991, **30**, 1980.
23 M. Süßner and H. Plenio, *Chem. Commun.*, 2005, 5417.
24 (*a*) S. Leuthäußer, V. Schmidts, C. M. Thiele and H. Plenio, *Chem.–Eur. J.*, 2008, **14**, 5465; (*b*) R. Credendino, L. Falivene and L. Cavallo, *J. Am. Chem. Soc.*, 2012, **134**, 8127.
25 L. Cavallo, A. Correa, C. Costabile and H. Jacobsen, *J. Organomet. Chem.*, 2005, **690**, 5407.
26 (*a*) F. C Courchay, J. C. Sworen and K. B. Wagener, *Macromolecules*, 2003, **36**, 8231; (*b*) T. M. Trnka and R. H. Grubbs, *Acc. Chem. Res.*, 2001, **34**, 18; (*c*) A. Fürstner, L. Ackermann, B. Gabor, R. Goddard, C. W. Lehann, R. Mynott, F. Stelzer and O. R. Thiel, *Chem.–Eur. J.*, 2001, **7**, 3236.
27 D. J. Nelson, S. Manzini, C. A. Urbina-Blanco and S. P. Nolan, *Chem. Commun.*, 2014, **50**, 10355.
28 (*a*) G. C. Vougioukalakis and R. H. Grubbs, *Chem.–Eur. J.*, 2008, **14**, 7545; (*b*) T. Vorfalt, K.-J. Wannowius and H. Plenio, *Angew. Chem., Int. Ed.*, 2010, **49**, 5533.
29 V. Thiel, M. Hendann, K.-J. Wannowius and H. Plenio, *J. Am. Chem. Soc.*, 2012, **134**, 1104.
30 F. Nuñez-Zarur, X. Solans-Monfort, L. Rodríguez-Santiago and M. Sodupe, *Organometallics*, 2012, **31**, 4203.
31 I. W. Ashworth, I. H. Hillier, D. J. Nelson, J. M. Percy and M. A. Vincent, *ACS Catal.*, 2013, **3**, 1929.
32 Substrate **9** and **13** were simulated by 4,4-dimethylpent-1-ene.
33 Substrate **17** was simulated by 2,4,4-trimethylpent-1-ene.

 